ELSEVIER

Journal of Nuclear Materials 241–243 (1997) 244–249

journal of nuclear materials

Section 2. ITER and reactor papers

Side radiation damage from ablated vapor following an ITER-scale disruption

A.E. Koniges [a,*], D.C. Eder [a], H.A. Scott [a], H. Würz [b], F. Kappler [b]

[a] *Lawrence Livermore National Laboratory, Livermore, CA 94550, USA*
[b] *Forschungszentrum, Karlsruhe, Germany*

Abstract

Disruptions and giant ELMs in ITER will deposit a large power load on the divertor plates. The amount of ablated material is important for plate lifetime and in determining the amount of plate material that escapes to the core region. The ablated vapor is effective at mitigating continued ablation via radiation shielding of the surface. Calculations in 1D have shown that the radiation, generated in the vapor following absorption of the energy from the core, is usually at least a factor of 10 more likely to leave the vapor in the direction of the core as compared to striking the divertor plate. However, the ablated vapor also emits in the direction of the side walls. We discuss the effect of this ancillary side radiation for two divertor designs. The 2D plasma profiles of temperature and density are modeled as a Gaussian fit to 1D data. These are used in a non-local thermodynamic equilibrium (NLTE) radiation transport code to give a detailed calculation of the side radiation. The radiation field is non-isotropic and couples regions with different densities and temperatures. We find that the side-wall radiation incident on different wall locations is comparable to the flux incident on the strike plate. Vapor shielding calculations are required to determine the amount of ablated material from these side-wall structures. Future 2D calculations of this type will aid in deciding the optimum divertor design for ITER.

Keywords: Disruptions; Plasma–wall interaction simulator; Divertor plasma; Physical erosion

1. Introduction

Vapor shielding is expected to play a significant role in reducing the ablation of the Be divertor strike plate during plasma disruptions for the next generation of fusion devices such as ITER. During a disruption a significant fraction of the stored thermal energy is channeled along the open flux surfaces and deposited on the strike plate in the divertor [1,2]. Initial ablation/evaporation of the surface results in a low temperature vapor which quickly has sufficient density along the field lines to absorb the energy of the incoming particles before they can strike the surface. This can reduce the subsequent ablation of the surface. The vapor is heated as energy is deposited by plasma ions and electron conduction and emits a large fraction of this energy as radiation. If the vapor is optically thick near the plate but optically thin in the lower density outer parts of the vapor, the radiation leaves the vapor preferentially in directions away from the plate and is directed throughout the divertor region and the subsequent ablation is reduced at the strike plate. Besides the strike point at the divertor plate, radiation emitted from the ablated plasma vapor may be energetic enough to affect damage on the divertor side walls. In this paper, we concentrate on estimating the side-wall radiation, which is a secondary effect following the strike-point material ablation. This calculation of the energy load on the side walls requires a 2D treatment of the radiation field in the ablated plasma.

A proposed strike material for ITER divertors is Be which will be at various degrees of ionization, e.g., H-, He-, or Li-like Be, in different portions of the ablated plasma. To accurately calculate the radiation from Be a detailed atomic model is required that includes all these different ionization stages. A significant fraction of the

* Corresponding author.

PII S0022-3115(96)00508-9

radiation is from bound–bound transition and these lines can have very different opacities than the surrounding continuum [3]. In particular, for some of the stronger lines a coupled calculation of line transfer and atomic kinetics is required to accurately predict the emitted radiation from the ablated plasma.

In this paper, we estimate the flux levels at the side walls from a Be plasma. The temperature and density profiles in the ablated Be plasma along the field lines are calculated using the 1D code FOREV-1 [4]. The transverse profile is approximated as a Gaussian. Thus at any given time in the FOREV-1 calculation, we can produce a 2D set of plasma conditions to be used as input into a non-LTE radiation transport code to give a detailed calculation of the radiation from the emitting plasma. Finally, calculations of the radiation flux at a series of points outside of the plasma corresponding to divertor wall locations are calculated. In Section 2, we describe the detailed NLTE radiation transport calculation. In Section 3, we give estimations of side wall flux levels and the values to plate and core.

2. 2D radiation transport

The 2D radiation problem is modeled using a NLTE simulation code [5]. The simulation code itself contains no atomic data. Instead, the level structure and transition processes for the particular element being studied are included as part of an atomic model, which is provided as input for the code along with temperature and density information. For Be we have constructed a detailed atomic model for the four ionization stages [3]. The model has a total of 123 levels with states having a principle quantum number $n \leq 4$ treated in detail. For states with $10 \geq n \geq 5$ there is one level for each principle quantum number. The model specifies the energy of each level and the rates that connect the levels. The atomic rates include electron–ion and ion–ion collisions, photo-ionization, photo-excitation, and Auger processes. The rates for inverse processes are done via detailed balance.

In general, the code is provided with time varying values of temperature and density on a 2D grid. In the current application, we are interested in a steady-state solution to the specified input obtained from the FOREV-1 code at a given time. In this case, the code starts with an initial assumption of LTE which specifies the initial atomic populations and the associated radiation field. Then, spatial coupling is introduced via radiation transport, and the atomic kinetics calculation is alternated with further radiation transport until a converged NLTE state is realized.

The radiation transport treats continuum and line radiation separately. The coupled line transfer/atomic kinetics calculation is done for a specified set of strong lines. The contribution from the remaining bound–bound transitions are included in the continuum transport. The line transfer is done using a ray-based algorithm derived from the formal integral solution to the transfer equation. The formal transfer equation is given by

$$\frac{\mathrm{d}I_\nu}{\mathrm{d}\tau_\nu} = I_\nu - S_\nu,$$

where I_ν is the specific intensity, S_ν the source function, and τ_ν the optical depth along the ray. The transfer equation may be integrated along a ray to obtain the formal solution

$$I_\nu(\tau_\nu) = I_\nu(0)\mathrm{e}^{-\tau_\nu} + \int_0^{\tau_\nu} S_\nu(t)\mathrm{e}^{-t}\mathrm{d}t.$$

With the assumption of complete redistribution (CRD), lines couple through the line strengths $\bar{J}^l$, defined as

$$\bar{J}^l = \int \frac{\mathrm{d}\Omega}{4\pi} \int \mathrm{d}\nu\, \phi_\nu^l I_\nu.$$

In two dimensions, the formal solution method used by the NLTE code is based on a so-called 'short characteristic' integration [6,7]. The ray nature of the radiation transfer equation specifies that photons are propagated downstream along a ray. To determine the radiation at a given mesh point along a ray, the intensity of the radiation entering the cell at the upstream end of the ray segment (the short characteristic) is required. This quantity can then be adjusted by the amount of radiation absorbed and emitted in the cell.

Consistency between atomic populations, source functions, and line intensities is achieved with a complete linearization procedure, which can handle overlapping and interacting lines [5,8]. This is required in optically-thick situations where all the quantities are coupled. The linearization procedure is independent of the formalism used to solve the transfer equation. A complete calculational cycle for the linearization consists of three steps: (1) evaluate the atomic populations, source functions, and the derivatives $\partial S_\nu / \partial \bar{J}^{l'}$ using the line strengths $\bar{J}^{(0)}$ calculated during the previous cycle; (2) perform the formal transfer calculating $I_\nu^{(0)}$; and (3) solve the linearized equations for $\Delta \bar{J}^l$ and update $\bar{J}^l = \bar{J}^{l(0)} + \Delta \bar{J}^l$. Because of the size of the linearization operator in two dimensions, an approximate operator formulation of the standard complete linearization algorithm is adopted [5].

3. Results

The 1D radiation magnetohydrodynamics code FOREV-1 is used to model the initial plasma ablation [4]. In FOREV-1, the three classical conservation equations for mass momentum and energy balance are solved. The energy balance equation is coupled with the equation for the 1D radiation transport and the momentum equation is coupled with the magnetic field diffusion equation. We

perform the radiation transport in two dimensions using plasma temperature and density profiles from the FOREV-I in the longitudinal direction and Gaussian in the transverse direction. The Gaussian is chosen to have full-width at half maximum of 5 cm.

In the radiation transport model we specify 30 transitions in Li-, He-, and H-like Be for self-consistent line transfer. Each line is strongly coupled to at least one other line. The remaining bound–bound transitions are done jointly with the continuum transfer calculation. The continuum is calculated with 235 energy bins. This binning structure was tested in one-dimension with up to 3 times the number of energy bins yielding no significant difference. Integration of the spectrum to yield the flux is performed with 8000 energy bins to account for the large number bound–bound transitions not explicitly included in the self-consistent line transfer. For each zone the radiation flux is calculated in approximately 60 directions. For zones along the edges of the 2D mesh, the flux is spatially integrated to determine the flux incident on the strike plate and flux emitted in other directions. We give results for the flux along the different edges of the simulation. To determine the flux at wall locations not in contact with the plasma, one requires more than the fluxes at the edge of the plasma because the emission is non-isotropic and information is lost during the spatial integration. For specified side wall locations, we calculated the incident flux using the angular dependent flux from all relevant edge zones. These sites are sometimes referred to as detector locations because the code allows for a specified acceptance solid angle and directionality.

In order to estimate the side-radiation damage for the ITER divertor designs, we choose a representative

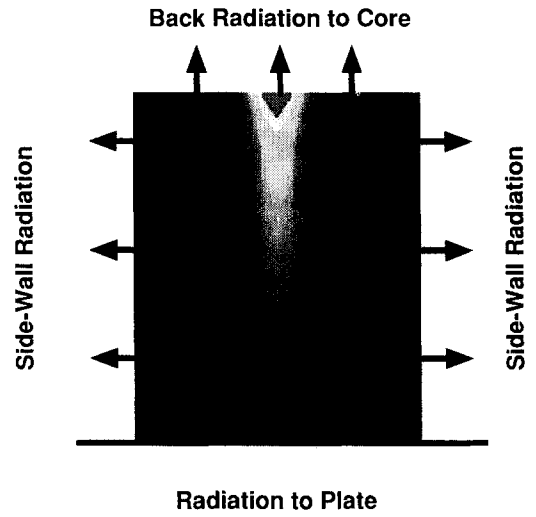

Fig. 2. Temperature contours used in 2D NLTE calculation with directions of side walls, plate and core shown.

FOREV-1 calculation for an incoming ion flux of 10 MW/cm^2. At a time of 100 μm in the ablation calculation, we use the temperature and density in the 16 zones to define the profiles in the direction along the field lines which are shown in Fig. 1. We use 5 zones in the transverse direction using a Gaussian profile with a FWHM of 5 cm. Advantage is made of the symmetry in the transverse direction so only one side of the transverse profile is used in the calculation. The NLTE atomic kinetic radiation transport is thus performed on a 5×16 mesh. The NLTE code is used to determine the radiation to the strike plate, the back radiation to the core, and the side-wall

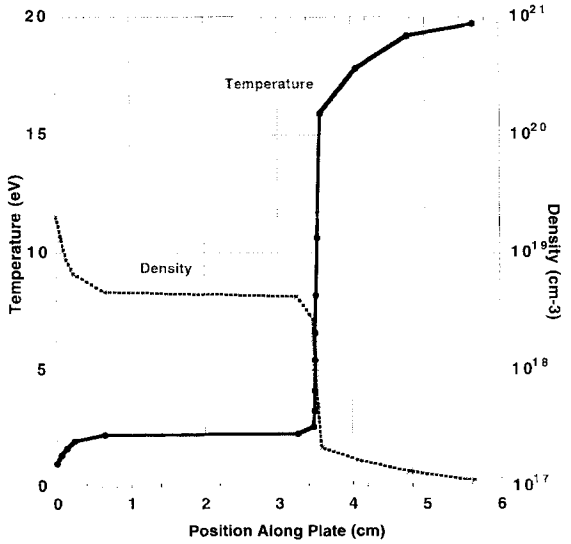

Fig. 1. Profiles of the temperature and density obtained from the FOREV-I calculation.

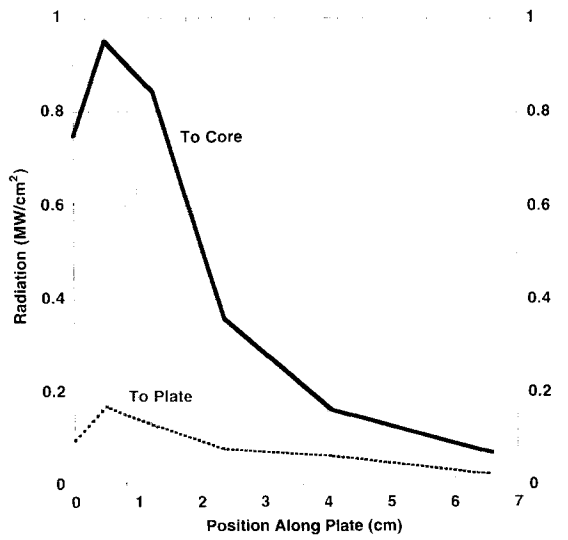

Fig. 3. Radiation normal to the surface along edges of plasma in direction towards core and plate, as shown in Fig. 2.

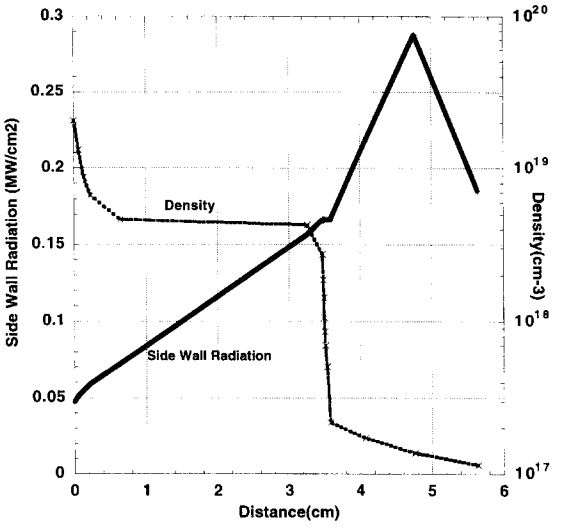

Fig. 4. Radiation along edge of plasma in direction towards side walls along with the maximum density as a function of distance away from the plate.

radiation. Temperature contours and the radiation direction of interest are shown in Fig. 2. We also did 1D NLTE calculations for these 16 zones and found radiation fluxes of 0.4 and 4.6 MW/cm^2, for the plate and core respectively. (If LTE is assumed, the values are 0.5 and 10.0 MW/cm^2.) The 2D results for these fluxes are shown in Fig. 3. The values are reduced as expected because of the finite transverse extent of the plasma. The peak value to the plate is approximately 0.2 MW/cm^2 or half the 1D value. The peak value to the core is approximately 1 MW/cm^2 or a bit less than one quarter of the 1D value. However, the effect of vapor shielding is clearly seen with the core values being significantly larger. The radiation along the edge of the plasma directed towards the side walls is shown in Fig. 4. The flux values are significantly less than those directed towards the core but somewhat larger than those directed towards the strike plate. The peak value is approximately 0.3 MW/cm^2 at a distance 5 cm away from the plate. The amount of side-wall radiation that strikes a side-wall location depends on its position relative to the ablated plasma. Figs. 5 and 6 show two different divertor designs proposed for ITER. The ablated plasma region is depicted as a slab along the magnetic flux lines. The separatrix is shown passing through the edge of

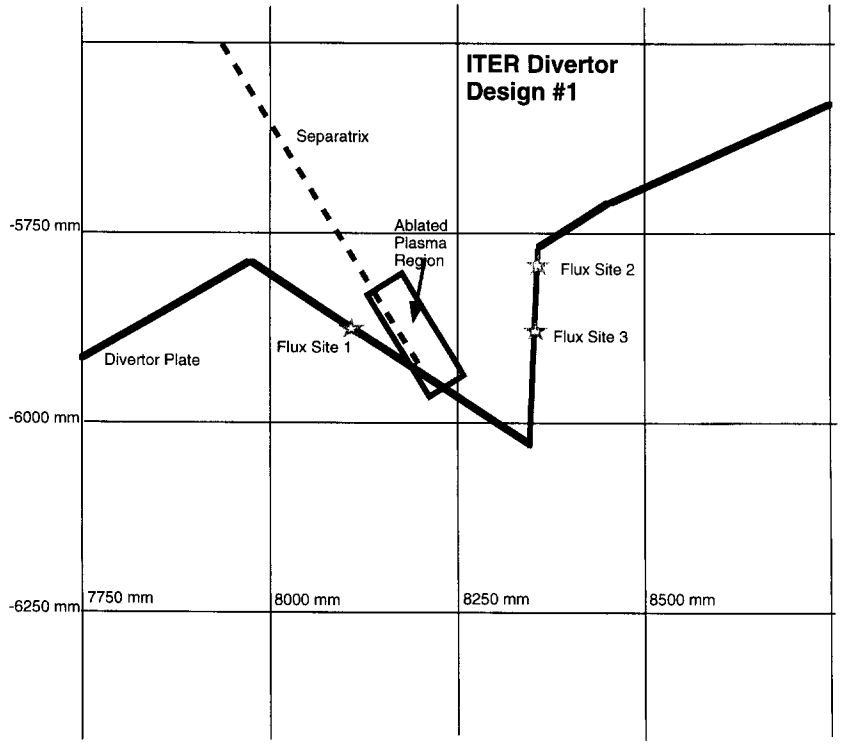

Fig. 5. One of the ITER divertor design configurations. Distances are shown in mm from the center of the vessel. Detailed calculations of incoming photon flux from the ablated Be plasma are calculated at each of the flux sites. The approximate strike point is located where the dotted line, which denotes the sepratrix, intersects the divertor plate. The initially ablated plasma is assumed inside the region of the rectangular box. This radiating plasma then emits energy which propagates to the side walls of the divertor. Here we have chosen representative flux sites and various distances from the ablated radiating plasma.

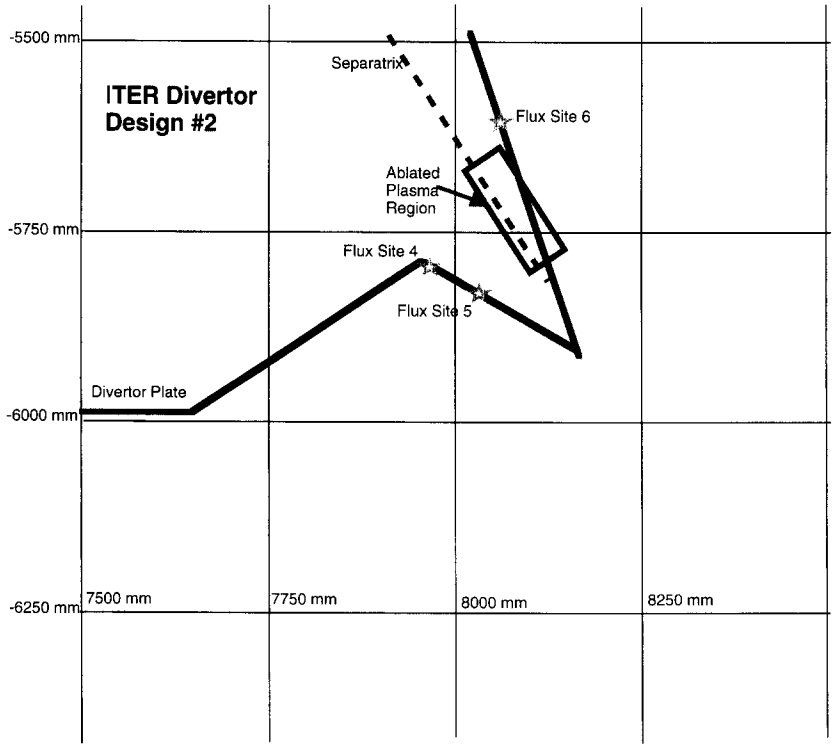

Fig. 6. Another one of the ITER divertor design configurations. Flux sites, etc. are chosen as in Fig. 5.

the plasma. In the model calculation, flux 'detectors' are placed at different sites along the divertor side walls. These positions are noted as stars in Figs. 5 and 6. Each detector calculates the incoming photon flux for a 2π acceptance solid angle. In Fig. 7 we show results for these detectors compared to the flux directed towards the strike plate. We find that the value of the flux at the different side-wall locations is generally smaller than that striking the divertor plate. Here, more detailed calculations should reveal the amount of ablated material in these regions and whether or not vapor shielding will be effective at the lower flux values.

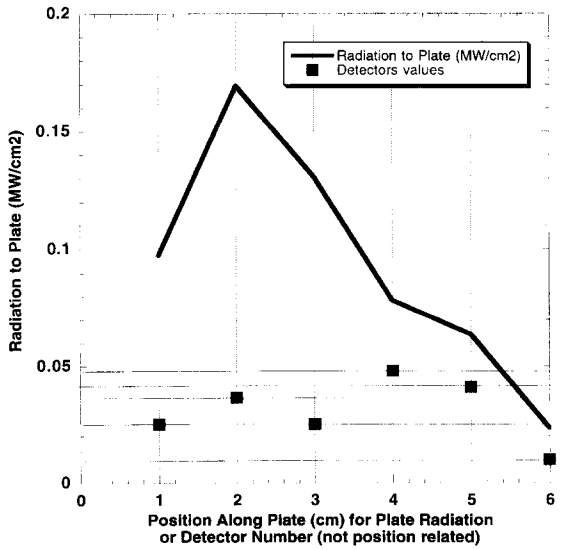

Fig. 7. Radiation at different detector values compared to values at the strike plate.

4. Summary

We find that the vapor shielding calculated in 1D is still effective in 2D with the majority of the radiation directed back towards the core and away from the strike plate and side walls. The radiation directed towards the side walls is somewhat smaller than that directed towards the strike plate. If side walls are near to the edge of the ablated plasma, heating and material removal from these surfaces must be considered. This is the case for both of the ITER divertor designs considered in this paper. It is clear that more work in this area is required including a comparison of radiation calculation using degrees of complexity.

Acknowledgements

This work was supported by US DOE at LLNL under contract W-7405-ENG-48 and by ITER US Home Team.

References

[1] D. Post, S. Cohen, J. Hogan, W. Nevins, P. Rutherford et al., Fus. Tech. 21 (1992) 1434.
[2] A. Hassanein and D. Ehst, J. Nucl. Mater. 196–198 (1994) 680.
[3] A.E. Koniges, D.C. Eder, A.S. Wan, H.A. Scott, H.E. Dalhed, R.W. Mayle and D.E. Post, J. Nucl. Mater. 220–222 (1995) 1116.
[4] H. Würz et al., presented at the 12th Int. Conf. on Plasma Surface Interactions, May 1996, St Raphaël, France.
[5] H.A. Scott and R.W. Mayle, Appl. Phys. B 58 (1994) 35.
[6] P. Kunasz and L. Auer, J. Quant. Spectrosc. Radiat. Transfer 39 (1988) 67.
[7] P. Kunasz and G. Olson, J. Quant. Spectrosc. Radiat. Transfer 39 (1988) 1.
[8] D.C. Eder and H.A. Scott, J. Quant. Spectrosc. Radiat. Transfer 45 (1991) 189.